Article:
Hepworth, C., Wood, W.H.J., Emrich-Mills, T.Z. et al. (3 more authors) (2021) Dynamic thylakoid stacking and state transitions work synergistically to avoid acceptor-side limitation of photosystem I. Nature Plants. ISSN 2055-026X

https://doi.org/10.1038/s41477-020-00828-3

Dynamic thylakoid stacking and state transitions work synergistically to avoid acceptor-side limitation of photosystem I

Christopher Hepworth[1], William H.J. Wood[1], Tom Z. Emrich-Mills[1], Matthew S. Proctor[1], Stuart Casson[1] and Matthew P. Johnson[1]

[1]Department of Molecular Biology and Biotechnology, University of Sheffield, Firth Court, Western Bank, Sheffield, S10 2TN, United Kingdom.

*=Corresponding author matt.johnson@sheffield.ac.uk

Abstract

TAP38/STN7-dependent (de)phosphorylation of light harvesting complex II (LHCII) regulates the relative excitation rates of photosystems I and II (PSI, PSII) (state transitions) and the size of the thylakoid grana stacks (dynamic thylakoid stacking). Yet, it remains unclear how changing grana size benefits photosynthesis and whether these two regulatory mechanisms function independently. Here by comparing *Arabidopsis* wild-type, *stn7* and *tap38* plants with the *psal* mutant, which undergoes dynamic thylakoid stacking but lacks state transitions, we elucidate their distinct roles. Under low light, smaller grana increase the rate of PSI reduction and photosynthesis by reducing the diffusion distance for plastoquinol, however this beneficial effect is only apparent when PSI/PSII excitation balance is maintained by state transitions or far-red light. Under high light, the larger grana slow plastoquinol diffusion and lower the equilibrium constant between plastocyanin and PSI, maximising photosynthesis by avoiding PSI photoinhibition. Loss of state transitions in low light or maintenance of smaller grana in high light also both bring about a decrease in cyclic electron transfer and over-reduction of the PSI acceptor-side. These results demonstrate that state transitions and dynamic thylakoid stacking work synergistically to regulate photosynthesis in variable light.

Introduction

Natural environments expose plants to large and rapid variations in light intensity[1]. These can cause mismatches between the rate of photosynthetic electron transfer and the capacity of downstream electron sinks, such as the CO_2-fixing Calvin-Benson-Bassham (CBB) cycle [2]. The build-up of electrons on the acceptor-sides of photosystems I and II (PSI and PSII) can damage the delicate reaction centres by promoting formation of reactive oxygen species (ROS)[3]. Fortunately, plants possess an extensive armoury of regulatory mechanisms, allowing them to cope with fluctuations in light intensity and avoid, or minimise, photo-oxidative stress. PSII is protected by non-photochemical quenching (NPQ), wherein excess absorbed solar energy in the light harvesting antenna complexes (LHCII) is safely dissipated as heat[4]. PSI is protected primarily by photosynthetic control, which avoids over-reduction of the acceptor-side by regulating the rate of electron donation from the cytochrome b_6f (cytb_6f) complex via plastocyanin (Pc)[5]. NPQ and photosynthetic control are induced in high light by the build-up of the transmembrane ΔpH that results from coupled linear and cyclic electron transfer (LET and CET)[4–6]. While LET involves transfer of electrons from water to $NADP^+$ via PSII, plastoquinone (PQ), cytb_6f, Pc, PSI, ferredoxin (Fd) and ferredoxin-$NADP^+$ reductase (FNR), CET recycles electrons from Fd back to the PQ pool, contributing to ΔpH and ATP synthesis without net $NADP^+$ reduction. In *Arabidopsis* Fd-PQ reductase (FQR) activity is associated with two separate pathways, the first involves photosynthetic complex I (NDH) and the second involves the PGR5 and PGRL1 proteins and is sensitive to the inhibitor antimycin-A (AA)[6,7]. PGR5 and PGRL1 have been suggested to function directly as the AA-sensitive FQR[8] or act as regulators of FQR activity by an FNR-cytb_6f complex[9,10]. Since ΔpH forms and relaxes on a timescale of seconds, NPQ and photosynthetic control are able to rapidly track light intensity[2,4,5]. In addition, plants can regulate photosynthesis by

60 modulating the redox state of the photosynthetic electron transfer chain via the reversible
61 phosphorylation of LHCII[11,12]. In contrast to photosynthetic control and NPQ, this
62 mechanism occurs on timescales of minutes to tens of minutes, so is likely to integrate
63 changes in light intensity and spectral quality over a longer period. The stromal-facing N-
64 terminii of the LHCB1 and LHCB2 subunits of LHCII are phosphorylated by the serine-
65 threonine kinase STN7 and dephosphorylated by the phosphatase TAP38 (PPH1)[13–15]. In low
66 light STN7 is activated by the binding of plastoquinol (PQH_2) to the oxidising site of the
67 cytb_6f complex[16]. In high light, STN7 is inactivated by the build-up of reduced thioredoxin in
68 the stroma and/or the ΔpH[17,18]. Since TAP38 is believed to be constitutively active, the
69 activity of STN7 thereby determines the steady state phosphorylation level of LHCII[14,15].
70 Loss of LHCII phosphorylation, NPQ or photosynthetic control is associated with reduced
71 plant growth and yield in fluctuating light, characteristic of natural environments[19–22].
72 When LHCII is dephosphorylated the majority is energetically coupled to PSII (State
73 I). Phosphorylation results in an increased proportion of LHCII becoming energetically
74 coupled to PSI via its PSAL/H/O subunits (State II)[23]. In this way phosphorylation regulates
75 the relative excitation rates of PSI and PSII to ensure efficient operation of the LET chain, a
76 mechanism known as the state transition[11,12]. Since State II increases PSI/ PSII excitation
77 ratio it was also suggested as a mechanism to increase the CET to LET ratio and therefore the
78 supply of ATP relative to NADPH[24–27]. It is clear however that CET does not obligatorily
79 depend on state transitions in either *Arabidopsis* or *Chlamydomonas*[28,29]. LHCII
80 phosphorylation also affects the organization of the thylakoid membrane by controlling the
81 interactions between the stromal faces of LHCII complexes that sustain grana stacking[30].
82 Phosphorylation in low light promotes a reduction in the number of membrane layers and
83 diameter of the grana stacks, while increasing the number of grana per chloroplast;
84 dephosphorylation in high light provokes the opposite response[31–34]. Unlike state transitions,

the function of dynamic thylakoid stacking is not well established. Smaller grana were suggested to facilitate the exchange of phosphorylated LHCII between grana and stromal lamellae[30]. Recent theoretical work showed that larger grana increase light scattering relative to absorption, thus potentially acting as a photoprotective mechanism in high light[35]. Using absorption flash spectroscopy, we recently demonstrated that reducing grana size increased the rate of PSI reduction in spinach, and suggested this could increase LET efficiency[33]. In contrast, we found that PSI reduction following far-red illumination was enhanced in larger grana, consistent with an increased capacity for CET[10,33]. We therefore hypothesised that dynamic thylakoid stacking could act as mechanism to control the CET to LET ratio, though in this case the dephosphorylated state would favour CET[33].

The absence of LHCII phosphorylation in the *stn7* mutant under low light conditions leads to an over-reduction of the PQ pool and acceptor-side limitation of PSII, reducing LET [36–38]. However, to date no obvious penalty has been demonstrated for the maintenance of LHCII phosphorylation in high light in the *tap38* mutant. Moreover, it remains unclear whether dynamic thylakoid stacking affects photosynthetic efficiency in the steady state and whether it can act independently of state transitions. In this study we compared the behaviour of wild-type (WT), *stn7* and *tap38 Arabidopsis* plants with the *psal* mutant, which lacks state transitions but retains dynamic thylakoid stacking, to better understand how LHCII phosphorylation regulates photosynthesis in low and high light.

Grana size and state transitions in WT, *psal, stn7* and *tap38*

Previously dynamic thylakoid stacking has been studied under broadband white light [31–33]*;* hence we first sought to establish if this phenomenon was also observable under the 635 / 460 nm light combination employed by the infra-red gas exchange, absorption spectroscopy and chlorophyll fluorescence instruments used in the following experiments. Using structured

illumination microscopy (SIM) we assessed grana size in low light (LL, 125 μmol photons m^{-2} s^{-1}) and high light (HL, 1150 μmol photons m^{-2} s^{-1}) (Fig 1A). The mean grana diameter, as measured by the full width half maximum (FWHM) of the fluorescence signal of each granum, was significantly smaller in WT, *psal* and *tap38* in LL compared to *stn7*, while in HL the *psal*, WT and *stn7* were larger than *tap38* (Fig 1B). Using 77K fluorescence emission spectroscopy we compared the relative antenna size change of PSI between LL and HL in WT and the mutants (Fig 1C). In the WT there is a decrease in the F735 (PSI)/F685 (PSII) fluorescence ratio between LL and HL conditions consistent with a State II to I transition as STN7 is inactivated in HL (Fig. 1C). However, no difference is seen in either *stn7* or *psal*, which remained locked in State I in both LL and HL with a low F735/F685 ratio and *tap38* that remained locked in State II (Fig. 1C)[13,14,23,39]. These differences in the relative PSI/PSII antenna size were confirmed using absorption and fluorescence spectroscopy (Extended Data Fig. 1).

Effect of grana size and state transitions on photosynthesis

We next used infra-red gas exchange and chlorophyll fluorescence imaging to assess the photosynthetic properties of the mutants in low light (LL, 125 μmol photons m^{-2} s^{-1}) and high light (1150 μmol photons m^{-2} s^{-1}). After 10 minutes of LL illumination, CO_2 assimilation ($^{A}CO_2$) was higher in WT and *tap38* compared to *stn7* and *psal* (Fig. 2A). On the other hand, in HL *tap38* showed significantly lower $^{A}CO_2$ than *stn7*, WT and *psal* (Fig. 2A). These effects were not due to differences in stomatal density or conductance, which were similar among the mutants and WT (Extended Data Fig. 2). Chlorophyll fluorescence imaging showed that the PSII quantum yield (ΦPSII) was lowest in *psal* and *stn7* in LL, while in HL it was lowest in *tap38* (Fig. 2B). While the inferior $^{A}CO_2$ and ΦPSII of *stn7* and *psal* in LL is expected [13,36,37], the inferior performance of *tap38* in HL has not, to our knowledge, been

previously reported. Using chlorophyll fluorescence and P700 absorption spectroscopy we next subjected plants to 10 minutes of LL illumination, briefly augmented for 30 seconds with far-red (FR) light (740 nm, 255 μmol photons m^{-2} s^{-1}) between the 400-430 second time points, followed by 10 minutes of HL, and finally 4 minutes of dark relaxation (Fig. 2C-H). The 30 seconds of FR is sufficient to reach a steady state level of P700 oxidation[40], but insufficient to reverse LHCII phosphorylation and cause reversion to State I, a process which takes ~15-30 minutes[11,12]. Under LL illumination the ΦPSII initially decreased in all plants, but then rose in the subsequent minutes as the CBB cycle and downstream electron sinks were activated and the transient NPQ relaxed (Fig. 2C and E). The NPQ transient was largest in *stn7* and smallest in *tap38* (Fig. 2E). ΦPSII was highest in *tap38* after ~100 seconds, while in subsequent 100-200 seconds the WT rose to the same level, consistent with the transition to State II. *Psal* and *stn7*, which are locked in State I, showed a ~20% lower ΦPSII, which did not increase further (Fig. 2C). Augmentation of LL with FR for 30 seconds transiently increased ΦPSII in *psal* to WT/*tap38* levels but had a significantly diminished restorative effect in *stn7* (Fig. 2C). The lower ΦPSII under LL in *stn7* and *psal* was accompanied by an increased reduction of the PSII acceptor Q_A (measured as 1-qL) compared to *tap38* and WT. This effect is likely caused by inefficient oxidation of the PQ pool by PSI (via cytb_6f) due to its under-excitation relative to PSII in the *stn7* and *psal* plants (Fig. 2D). Consistent with this idea augmentation of LL with FR lowered 1-qL in *psal* and *stn7*, however the effect was smaller in the latter (Fig. 2D). Since the level of PSI and Pc:PSI ratios are similar in *psal* and *stn7* (Extended Data Fig. 3) their differential performance in LL + FR indicates that the latter has some additional disadvantage that cannot be corrected by boosting PSI excitation. As in PSII, the PSI quantum yield (ΦPSI) transiently decreased when LL illumination commenced, and this was coincident with a transient rise in the PSI donor side limitation (Y(ND)) (Fig. 2F and G). ΦPSI rose as the CBB cycle was activated and was highest in *tap38*; by 250 seconds

160 the WT rose to a level not significantly different (Fig. 2F). Rising ΦPSI in all plants was
161 mirrored by a decrease in the PSI acceptor side limitation (Y(NA)) (Fig. 2H). The ΦPSI and a
162 Y(NA) values in the *stn7* and *psal* mutants began to diverge gradually from the wild-type
163 from 250 s onwards during the LL period and after ~400 s they were significantly different
164 (Fig. 2F and H). Increased Y(NA) in *stn7* relative to WT agrees with previous observations
165 made in low and fluctuating light[36]. FR decreased the ΦPSI in all plants but simultaneously
166 decreased Y(NA), while Y(ND) increased (Fig. 2F, G and H). This effect is in line with the
167 preferential excitation of PSI with FR, which oxidises the inter-system electron transfer chain
168 inducing a donor-side limitation. While ΦPSI falls under FR, the additional excitation will
169 nonetheless stimulate the rate of PSI electron transfer [41]. Notably, in *stn7* the Y(ND) is higher
170 under LL + FR than in *psal* (Fig. 2G). Therefore, only when the limitation of PSI oxidation
171 rate in LL is lifted by state transitions or FR augmentation can a beneficial effect of smaller
172 grana be observed.
173 The lower $^{A}CO_2$ and ΦPSII in *tap38* under HL (Fig. 2A-C) was accompanied by a
174 ~30% reduction in the level of rapidly relaxing NPQ (qE) compared to *stn7* (Fig. 2E). The qE
175 in the WT and *psal* started at a level similar to *tap38* when the light intensity is first
176 increased, before gradually transitioning to a level closer to the *stn7* over the course of 10
177 minutes (Fig. 2E). While 1-qL was lower in *tap38* under LL, in HL this mutant showed the
178 highest 1-qL, with WT, *stn7* and *psal* plants all significantly lower, consistent with their
179 higher qE (Fig. 2D and E). Likewise, ΦPSI under HL in *tap38* was significantly lower than
180 *stn7*; with WT and *psal* lying in between (Fig. 2F). Correspondingly in *tap38*, Y(ND) was
181 also significantly lower and Y(NA) higher than in *stn7* after the first 150 seconds of HL (Fig.
182 2G,H). Therefore, *stn7* and *tap38* plants show the opposite behaviour in LL and HL, with
183 LHCII phosphorylation promoting lower Y(NA) in LL and dephosphorylation promoting
184 lower Y(NA) in HL. If a smaller PSI antenna size was beneficial in HL then one would

185 expect *psal* to show a similar ΦPSII compared to *stn7* immediately upon transition from LL
186 to HL. Instead *psal*, like the WT, takes ~8-10 minutes to reach the higher ΦPSII and NPQ
187 and lower 1-qL levels in HL; a timescale consistent with dephosphorylation of LHCII and the
188 transition to larger grana (Fig. 2C-E)[32].
189
190 **Influence of grana size and state transitions on ET kinetics**
191 We investigated the difference in ΦPSII between *psal* and *stn7* in LL + FR and reduced
192 efficiency of *tap38* in HL further using dark interval relaxation kinetic (DIRK) analysis of
193 P700, Pc and Fd absorption (Fig. 3)[42,43]. In these DIRK experiments plants were treated for
194 10 minutes with LL (Fig. 3A), LL + FR (Fig. 3B) or HL (Fig. 3C) to reach the steady state,
195 then illumination was terminated and the ensuing kinetics of Pc and P700 reduction and Fd
196 oxidation were analysed. The LL + FR condition involved 9.5 minutes of LL with the final
197 30 seconds augmented with FR. In LL P700 remained reduced in all plants, while Pc, owing
198 to its lower redox potential, was partially oxidised[40,44]. In the WT and *tap38* Pc oxidation
199 reached 48% but only 30% in *psal* and *stn7* (Fig. 3A). Lower steady state Pc oxidation in LL
200 is consistent with the lower PSI activity in *psal* and *stn7* as they are locked in State I. In line
201 with the higher Y(NA) in *stn7* and *psal* in LL (Fig. 2H), the steady state Fd reduction level
202 was ~30% compared to ~20% in *tap38* and the WT (Fig. 3A). In LL + FR Pc oxidation level
203 increased to ~60% in WT, *tap38*, *psal and stn7* (Fig. 3B). In contrast under LL + FR, P700
204 oxidation was slightly higher at 25% in *stn7* compared to 18-20% in *psal*, WT and *tap38*
205 (Fig. 3B), consistent with the larger Y(ND) observed under these conditions (Fig. 2G). Fd
206 reduction was decreased in LL + FR compared to LL in all plants, although was still higher in
207 *stn7* than in WT and *tap38*, while *psal* was now similar to the latter pair (Fig. 3B). In HL Pc
208 oxidation was ~85% and P700 ~75% in WT, *stn7* and *psal*, however in *tap38* P700 was
209 ~60% oxidised and Pc ~98% oxidised (Fig. 3C). Fd in turn was more reduced in HL in *tap38*

(~40%) compared to *stn7,* WT and *psal* (~30%). Therefore, in HL Pc is more oxidised, whereas P700 and Fd are more reduced in *tap38* compared to *stn7*, WT and *psal* (Fig. 2E, G, H and Fig. 3C). This variation in the relationship between the fraction of Pc, P700 and Fd that are oxidised or reduced indicates that the equilibrium constant between these species is altered in *tap38* compared to *stn7*, WT and *psal.* This idea is explored further in Fig. 4 below.

The dark relaxation kinetics were next fitted with a single-exponential decay function to obtain the half-time (Extended Data. Fig 4)[45]. In LL + FR the half-time for $P700^+$ reduction ($P700^+_{red}$ t½) was ~20% shorter for *tap38*, WT and *psal* compared to *stn7* (Fig. 3D). In HL $P700^+_{red}$ t½ increased by ~20% in the WT and *psal* relative to LL + FR, whereas *stn7* and *tap38* did not show a significant change (Fig. 3D). Thus, $P700^+_{red}$ t½ remained significantly shorter in *tap38* in HL compared to *stn7*, WT and *psal* plants (Fig. 3D). A similar picture emerged from analysis of the Pc^+ half-time (Pc^+_{red} t½) with lower values for the WT, *psal* and *tap38* than *stn7* in LL and LL + FR (Fig. 3E). Under HL, the Pc^+_{red} t½ increased to a similar level in the WT and *psal* as in *stn7*, while in *tap38* it remained significantly shorter (Fig. 3E). Under LL, Fd^- oxidation (Fd^-_{ox} t½) half-time was shorter in the WT and *tap38* compared to *stn7* and *psal*, whereas in LL +FR *psal* was similar to WT and *tap38,* while *stn7* still lagged behind (Fig. 3F). Under HL, the Fd^-_{ox} t½ decreased compared to LL and LL + FR in all plants, although the decrease was significantly smaller in *tap38* (Fig. 3F). Increased Y(NA) in *tap38* under HL and *stn7* and *psal* under LL (Fig. 2H) is therefore accompanied by a longer Fd^-_{ox} t½ (Fig. 3F).

We calculated the initial rate of $P700^+$ and Pc^+ reduction and Fd^- oxidation by fitting the first 3-8 ms seconds of the DIRK with a linear function (Extended Data Fig. 4)[43]. In HL the rate of $P700^+$ and Pc^+ reduction was higher in *tap38* than WT, *stn7* and *psal* (Fig. 3C, E and H). In contrast, under LL+FR Pc^+ and $P700^+$ reduction rates were slower than in HL and now WT, *psal* and *tap38* were similar and faster than *stn7* (Fig. 3G, H). Under LL, Pc^+

reduction rates were fastest in WT and *tap38*, followed by *psal* and then slowest was *stn7* (Fig. 3H). Faster Pc^+ and $P700^+$ reduction in *tap38* under HL could be explained by the diminished photosynthetic control (Fig. 2G). However, smaller grana in *tap38, psal* and WT also increased the rate of reduction of Pc^+ relative to *stn7* under LL conditions, where photosynthetic control is absent (Fig. 3H). Under LL the initial rate of Fd^- oxidation was faster in *tap38* and WT compared to *psal* and *stn7*; *psal* was rescued by FR augmentation, whereas in *stn7* it remained slower (Fig. 3I). Under HL *tap38* showed slower Fd^- oxidation rate despite the higher steady state reduction owing to the longer Fd^-_{ox} t½ (Fig. 3C, F and I). Increased Y(NA) in *stn7* under LL and *tap38* under HL is therefore accompanied by a decrease in Fd^- oxidation rate, which may reflect a lower activity of either or both CET and the CBB.

Distinguishing the contributions of ΔpH and grana size

The increase in $P700^+_{red}$ and Pc^+_{red} t½ seen in the WT in HL (Fig. 3D and E) is consistent with photosynthetic control of the cytb_6f complex by ΔpH in HL[10,46,47]. The negligible increase in these parameters in HL for *tap38* may therefore indicate a reduced ΔpH in this mutant, which would be in line with the lower qE and Y(ND) (Fig. 2E, G). Measurement of the proton motive force (*pmf*) using electrochromic shift (ECS) absorption spectroscopy[48,49] confirmed that the *pmf* was lower in *tap38* in HL compared to *stn7* and *WT* (*psal* was not determined) (Fig. 4A). In contrast, under LL the *pmf* was slightly, but not significantly, lower in *stn7* compared to WT and *tap38* (Fig. 4A). The assignment of the relative partitioning of the *pmf* into ΔΨ and ΔpH using the ECS method remains controversial[50]. Nevertheless, using this method did not yield any differences in the partitioning of the components between WT, *tap38* and *stn7* in HL that might explain the differences (Extended Data Fig. 5A). Indeed, the only difference observed when this method was applied was a smaller ΔpH and higher ΔΨ in

WT under LL compared to *tap38* and *stn7*. Thus, the increased Pc^{+}_{red} t½ observed in *stn7* under LL cannot be ascribed to either a higher proportion of ΔpH or total *pmf*. Using a single-turnover flash over a FR background to pre-oxidise PSI, we measured $P700^{+}_{red}$ t½ in a range of grana size mutants (Fig. 4B). The values for the grana size in each mutant are calculated from previously reported SIM data [32]. We found a linear positive correlation (slope = 5.197, $r^2 = 0.9$) between grana size and $P700^{+}_{red}$ t½, with the highest values seen for the *curt1abcd* mutant that has ~1.35 μm diameter grana and the lowest for the CURT1A overexpressor (~0.3 μm) (Fig. 4B) [32,51]. These data indicate that $P700^{+}_{red}$ t½ may be affected by grana diameter as well as ΔpH. If Pc diffusion is affected by grana diameter then one would expect an effect on the redox equilibration between Pc and P700. The equilibrium constant (K_{eq}) for the forward reaction between the P700/$P700^{+}$ and Pc/Pc^{+} redox couples is ~81[55]. Compared to K_{eq}, an apparent equilibrium constant (K_{app}) of 13.1 was found for the WT under LL + FR conditions (Extended Data Fig. 5B) and just 4.4 under HL conditions (Fig. 4C). This value is much lower than K_{eq}, but in line with previous studies which show there is substantial disequilibrium between Pc and P700 *in vivo* and that K_{app} declines with increasing electron flux[44,52–55]. There was no significant difference in K_{app} values between the mutants in LL + FR conditions (Extended Data Fig. 5B). In contrast in HL, the K_{app} values were significantly different, with *tap38* giving the highest K_{app} and *stn7* the lowest, while WT and *psal* lay in between (Fig 4C). Therefore differences in Pc/P700 equilibration between *tap38* and *psal,* WT and *stn7* can explain some of the difference observed in $P700^{+}$ t½ under HL, but not under LL. Previously the Pc-P700 K_{app} was changed upon dark to light transition and attributed to an alteration in lumen thickness[53]. Using thin-section electron microscopy on LL and HL adapted leaves we examined lumenal sizes under HL and LL, but no significant difference was observed in the WT (Extended Data Fig. 6). Moreover, there was no significant difference between the mutants and WT in HL (Extended Data Fig. 6). These

results suggest that differences in K_{app} in HL between WT and the mutants are not due to altered lumen thickness. No differences were found in cytb_6f content between the mutants (Extended Data Fig. 7) that might explain the differences either. Another possibility is that the distribution of cytb_6f between the grana and stromal lamellae is affected by the LL and HL treatment, but no significant differences were observed between the mutants (Extended Data Fig. 7). The Pc:PSI ratio was lower in *stn7* and *psal* than WT and *tap38* (Extended Data Fig. 3), although since K_{app} was similar in WT and *psal* it suggests that grana size is the dominant factor. Another possibility is that grana size affects PQ/PQH_2 diffusion in the densely crowded thylakoid, which are ~70-80% protein by composition [56,57]. To investigate this further we subjected LL-adapted WT, *tap38* and *stn7* leaves to a 200 ms saturating flash and followed the subsequent re-oxidation of Q_A^- in the dark (Fig. 4D). For Q_A^- to be re-oxidised, PQ must bind to the Q_B-site of PSII. After the flash, PQ is regenerated by oxidation of PQH_2 at the oxidising site of cytb_6f. In *stn7* the half-time of Q_A^- re-oxidation ($Q_A^-{}_{ox}$ t½) is significantly increased compared to *psal*, *tap38* and WT in LL-adapted leaves, consistent with a retarded diffusion of PQH_2 between PSII and cytb_6f in this mutant (Fig. 4D). However, HL treatment increased $Q_A^-{}_{ox}$ t½ of the *psal*, WT to a similar level as *stn7,* although *tap38* was still faster (Fig. 4D). Therefore, the differences in PQ/PQH_2 diffusion can explain the variation in the $P700^+_{red}$ t½ LL+FR and part of that in HL, while differences in Pc diffusion/ equilibration also contribute to the differences in HL.

Influence of grana size and state transitions on CET

Since the Y(NA) phenotype of *stn7* under LL and *tap3*8 under HL were similar, we probed this parameter in more detail across a range of light intensities and found a cross-over at ~800 µmols photons m^{-2} s^{-1} (Fig. 5A). At light intensities below this value *tap38* shows lower Y(NA) than *stn7,* while above this intensity the opposite is true. In contrast the WT Y(NA)

310 remains comparatively low under all conditions (Fig. 5A) [40,58,59]. We investigated whether
311 HL treatment resulted in detectable damage to PSI by assessing the ECS a-phase amplitude in
312 leaves infiltrated with DCMU. Compared to dark-adapted leaves HL treated leaves showed
313 no-significant reduction in functional PSI for *stn7* and WT, however *tap38* showed a
314 significant reduction of ~10-15%, confirming PSI suffers light induced damage in this mutant
315 (Extended Data Fig. 8A).

316 We next compared the difference in estimated PSI and PSII electron transfer rates
317 inferred by chlorophyll fluorescence and P700 absorption spectroscopy respectively against
318 light intensity (ΔETR(I) = ETR(I)-ETR(II)), with excess PSI turnover reflecting the
319 contribution of CET and/or PSI charge recombination (Fig. 5B)[60–62]. The estimated ETR(I)
320 and ETR(II) values were corrected for each mutant based on the partitioning of light between
321 the photosystems determined by their relative antenna sizes (Extended Data Figure 1) and the
322 absorptivity of each leaf measured using an integrating sphere. In the WT ΔETR(I) increases
323 from 0 to ~600 μmols photons m^{-2} s^{-1} before declining slightly between 600 and 1500 μmols
324 photons m^{-2} s^{-1} (Fig. 5B). Infiltration of the WT with 1 mM methyl viologen, a PSI electron
325 acceptor that abolishes CET, suppressed ΔETR(I) at all but the lowest light intensities (Fig.
326 5B). In comparison to *stn7*, the ΔETR(I) for *tap38* was significantly higher at light intensities
327 below 250 μmols photons m^{-2} s^{-1}, although markedly lower at light intensities above ~600
328 μmols photons m^{-2} s^{-1} (Fig 5B). The data suggest that *stn7* and WT plants have increased
329 CET capacity in HL relative to *tap38*, and that *tap38* has a higher capacity under LL (Fig.
330 5B). We tested this idea further by infiltrating leaves with the CBB cycle inhibitor
331 iodoacetamide (IA), which irreversibly modifies sulfhydryl groups inactivating the CBB
332 cycle enzymes [63]. It has been shown previously that IA insulates the CET system against
333 electron loss, allowing the activity of the cyclic system to be measured with FR
334 illumination[63]. We found no difference in gH^+ between the mutants that might suggest a

differential sensitivity to IA (Extended Data Fig. 8B). Leaves of WT and *stn7* plants infiltrated with 4 mM IA and illuminated with FR showed higher levels of *pmf* than *tap38,* consistent with the higher capacity for CET (Fig. 5C), under conditions where the electron transfer chain is largely reduced[63]. Finally, we tested the idea that higher Y(NA) in LL in *stn7* and in HL in *tap38* is due to a smaller electron sink capacity by comparing leaves infiltrated with either 20 mM Hepes pH 7.5, 150 mM sorbitol, 50 mM NaCl (buffer) or buffer with NaCl replaced by 50 mM $NaNO_2$. The NO_2^- ion is reduced in the chloroplast stroma into NH_4^+, thus consuming electrons and potentially boosting the electron sink capacity. $NaNO_2$ caused a marked reduction in Y(NA) in *stn7* under LL and in *tap38* under HL relative to the buffer control lowering this parameter to WT levels in each case (Fig. 5D). We tested whether NO_2^- reduction in the chloroplast led to uncoupling through accumulation of NH_4^+ in the chloroplast by comparing the levels of rapidly-reversible ΔpH dependent NPQ (qE) in $NaNO_2$ versus buffer infiltrated leaves (Extended Data Fig. 8C). In fact, the results showed that NO_2^- slightly enhanced qE, probably due to higher LET, suggesting accumulation of NH_4^+ is insufficient to cause significant uncoupling.

Discussion

Dynamic thylakoid stacking adjusts membrane architecture to changes in light intensity and spectral quality, yet its exact function has remained unclear[30–34]. We previously observed that changing grana diameter affected $P700^+_{red}$ t½ in flash absorption spectroscopy experiments[33]. Here we observed the same in the steady state using DIRK; P700 reduction was faster when grana are smaller and slower when grana were larger. Control of $P700^+_{red}$ t½ by ΔpH - dependent regulation of the rate of PQH_2 oxidation by cytb_6f is well established[45,46,64]. However, since grana diameter affected $P700^+_{red}$ t½ under LL, where ΔpH is small and indistinguishable between *tap38* and *stn7*, as well as in HL, its effect is independent and

360 additive. Changes in the relative levels of cytb_6f and its lateral distribution between mutants
361 can be excluded as possible causes since these were not detected. The impact of grana
362 diameter on LET is further corroborated by its positive linear correlation with $P700^+_{red}$ t½ that
363 we observe in the single-turnover flash experiments (Fig. 4B). In principle, faster reduction
364 of $P700^+$ may result from faster Pc or PQ/PQH_2 diffusion within the membrane. Under LL,
365 $Q_A^-{}_{ox}$ t½ was significantly shorter in WT, *tap38* and *psal* plants with smaller grana than in
366 *stn7* with larger grana. This finding is consistent with previous reports comparing low light
367 and dark-adapted thylakoids and spinach leaves which showed that PQ/PQH_2 migration
368 within the membrane primarily occurs within nanodomains in the grana and that diffusion
369 between grana and stromal lamellae is much slower [56,65,66]. We suggest under conditions
370 where the PQ pool is relatively more oxidised, competition between PQ and PQH_2 for
371 binding the oxidising site of cytb_6f can limit LET [67]. Shortening the diffusion distance from
372 granal PSII to stromal cytb_6f via smaller grana would ameliorate this by effectively increasing
373 the concentration of cytb_6f involved in LET. However, we found this beneficial effect of
374 smaller grana under LL is only realised in steady-state measurements when the limitation on
375 P700 oxidation is first removed by state transitions or FR augmentation. Therefore, the
376 advantage of *psal*, which possesses smaller grana in LL but is locked in State I, over *stn7*
377 which possesses large grana and is locked in State I is only seen under FR illumination (Fig.
378 2C). Under HL, in addition to altered PQ/PQH_2 diffusion evidenced by a lower $Q_A^-{}_{ox}$ t½ in
379 *tap38* compared to the WT, *stn7* and *psal* (Fig. 4D), Pc diffusion also appears to play a
380 significant role. A clear difference is seen in Pc-P700 K_{app} between the mutants, with *tap38*
381 showing significantly higher K_{app} compared to *stn7,* WT and *psal* (Fig. 4C). Lower Pc-PSI
382 K_{app} could either reflect altered Pc/PSI ratios or slower diffusion between Pc and PSI due to
383 increased distance between granal cytb_6f and stromal PSI[33,55] or a narrower lumen[53]. A
384 decreased Pc/PSI ratio is observed in *stn7* and *psal*, however since the latter behaves like WT

385 in both LL and HL this change appears to have little effect. The relative insensitivity of K_{app}
386 to Pc/PSI ratio is consistent with the higher accumulation of Pc in in *Arabidopsis* compared
387 to other species where Pc levels correlate well with LET capacity[68]. Indeed, a 80-90%
388 decrease in Pc levels due to PETE2 knock-out in *Arabidopsis* had little effect on LET[69].
389 Since lumen width was not significantly different between the mutants, alterations in grana
390 diameter are implicated in variations in $K_{app,}$ consistent with recent results on the *curt1abcd*
391 mutant[55]. Interestingly, little change in K_{app} is observed between the mutants under LL
392 conditions. Therefore, the effect of increased grana diameter on Pc diffusion and Pc-P700
393 equilibration may only be felt under HL conditions when the high-potential chain is oxidised.
394 The benefit of larger grana to steady state LET rate can be clearly seen by comparison of *psal*
395 and *stn7,* in the former the transition to higher ΦPSII is gradual (Fig. 2C) despite this mutant
396 already being in State I. Therefore a smaller PSI antenna size in HL does not appear to
397 provide a benefit to LET efficiency, a finding compatible with the fact that P700 is a strong
398 excitation quencher irrespective of its redox state and is thus unlikely to be damaged by over-
399 excitation[70].

400 Remarkably, the symptoms of lower $^{A}CO_2$ and ΦPSII in *stn7* under LL and *tap38*
401 under HL were similar, both showing an over-reduction of the PSI acceptor side (Fig. 5A). In
402 the case of *tap38* this translated into damage to PSI upon prolonged 2 hour HL treatment
403 (Extended Data Fig. 8A). In the steady state, Y(NA) is maintained in the WT at a low level
404 (< 0.2) and the Fd pool redox state shows a consistent reduction of ~25-30% under both LL
405 and HL conditions (Fig. 3A-C), in line with recent reports[40,71]. Clearly the Fd redox state is
406 quite tightly controlled within narrow limits in the steady state (Fig. 3F). An increase in
407 Y(NA) i.e. the accumulation of electrons on the acceptor side of PSI reflects a mismatch
408 between the rate of Fd oxidation (Fig. 3I) and the rate of its reduction by PSI. Consistent with
409 this Y(NA) could be lowered in *stn7* under LL and *tap38* under HL by infiltration of leaves

410 with nitrite, which acts as an electron acceptor in the chloroplast stroma (Fig. 5D). The
411 balance between Fd oxidation and reduction is regulated at the PSI acceptor-side by the
412 activity of downstream electron sinks such as the CBB cycle and CET, and at the PSI donor-
413 side by photosynthetic control[72]. This normal pattern of PSI acceptor-side regulation is
414 disrupted when state transitions in LL and/ or transition to increased grana size in HL are lost.
415 How much of these mutant phenotypes can be explained by mis-regulation of LET alone or
416 by CET (with subsequent effects on LET) deserves consideration. On one hand in *tap38*
417 under HL, the higher Y(NA) could be explained by a partial loss of photosynthetic control
418 due to lower ΔpH (Fig. 4A), faster PQH_2 diffusion and a higher Pc-PSI K_{app} (Fig. 4C).
419 Similarly, in *stn7* under LL the higher Y(NA) could reflect an increased rate of LET that is
420 mismatched with the capacity of the CBB cycle to consume electrons. However, in our view
421 this 'LET only' explanation is inconsistent with several elements of our data: i) in *stn7* under
422 LL both ΦPSII and $^{A}CO_2$ are lower confirming that LET is inhibited rather than enhanced; ii)
423 the ability of FR light to decrease Y(NA) and increase LET under LL, iii) in *tap38* under HL
424 and in *stn7* under LL we observe a decrease in ΔETR(I), indicating lower CET capacity, in
425 each case (Fig. 5B).
426 An alternative more consistent with the data is therefore a combined 'LET *and* CET'
427 explanation i.e. we suggest that both photosynthetic control *and* acceptor-side regulation
428 through CET both play a role in the observed Y(NA) phenotype. This idea is further
429 corroborated by the recent work of Shikanai and co-workers who found the higher Y(NA)
430 observed in the *pgr5* mutant involved mis-regulation of both donor- and acceptor-side
431 regulation[58]. The ability of CET to limit Y(NA) is based on its ability to augment ΔpH
432 production by LET. The 'extra' ΔpH can be utilised by the ATP synthase to increase ATP
433 concentration in the stroma. The CBB requires 1.5 ATP/ NADPH, which given the 4.67
434 H^+/ATP ratio inferred by the structure of the chloroplast ATP synthase indicates a ATP

435 shortfall of ~0.32 ATP/ NADPH from LET alone[73]. The situation is complicated by the
436 multitude of other metabolic process in the stroma consuming ATP and NADPH in different
437 ratios[72], however the flexibility in the provision of ATP relative to NADPH provided by CET
438 appears to be crucial to plant fitness[74]. Thus, the high Y(NA) phenotype of *stn7* under LL and
439 *tap38* under HL could be explained by a shortfall in ATP due to lower CET that in turn leads
440 to a reduced CBB activity. The resulting slower regeneration of $NADP^+$ would of course also
441 lead to decreased ΦPSII, as is observed. A requirement for CET generated ΔpH to augment
442 ATP levels for maximising CBB cycle activity seems more likely in LL where *pmf* is non-
443 saturated (Fig. 4A). However, under HL there is evidence that substantial disequilibrium
444 exists between *pmf* and the phosphorylation potential[75,76], thus here CET may serve a purely
445 regulatory role both removing electrons form the PSI acceptor-side and downregulating the
446 donor-side through ΔpH production. This would be consistent with the higher *pmf* in *stn7*
447 compared to *tap38* under HL, but no reciprocal effect in LL (since additional *pmf* in *tap38* is
448 consumed through ATP production) (Fig. 4A).

449 What is the cause of lower CET in *stn7* under LL and *tap38* under HL? Saliently, we
450 observed that under LL conditions Y(NA) and Fd reduction level can be lowered and ΦPSII
451 increased by augmentation of PSI excitation with FR light in *psal* and *stn7* (Fig. 2C, H and
452 Fig. 3B). This effect was largely missing in *tap38* and WT plants, which adopt State II in LL
453 conditions (constitutively in the case of *tap38*). Increasing PSI excitation will increase the
454 ratio of PSI to PSII turnover, and thus CET relative to LET. Thus in LL, under-excitation of
455 PSI would appear to be the primary cause of lower CET, consistent with previous data in
456 plants and Chlamydomonas linking transition to State II with increased CET capacity[24–27].
457 Alternatively, to lower CET in LL, the smaller restorative effect of FR light on ΦPSII in *stn7*
458 compared to *psal* (Fig. 2C), may be explained by the slower PQ/PQH_2 diffusion in the former
459 due to its larger grana size (Fig. 4D). Indeed, this effect would likely mitigate the stimulatory

460 effect of FR by slowing both LET and CET, thus lowering the amount of extra ATP synthesis
461 it provokes. Under HL, CET no longer appears to be limited by PSI excitation since ΔETR(I)
462 it smaller in *tap38* despite the fact it possesses the largest PSI antenna (Fig. 5B, Extended
463 Data Fig. 1). Instead, we observed that in all plants the ΔETR(I) is increasingly suppressed as
464 light intensity increases, although the extent of suppression is greatest in *tap38* (Fig 5B). This
465 suppression is consistent with the experimentally demonstrated requirement of CET for redox
466 poise [52,63,77]. Previously, we obtained evidence that the larger grana observed in HL can assist
467 CET by slowing the reduction of the stromal PQ pool by PSII thus maintaining proper redox
468 posing of the CET pathway [33]. A similar effect of PQ compartmentalisation between grana
469 and stromal lamellae was previously observed by Joliot et al[65]. Thus, under HL CET is likely
470 limited by availability of oxidised PQ in the stroma. Here we provide further evidence for
471 this view showing that under HL ΔETR(I) is higher in both *stn7* and WT, where grana are
472 larger relative to *tap38*. It is striking that the symptoms of *tap38* in HL are a milder version of
473 those reported for *pgr5* mutant, which is compromised in the major CET pathway[74]. Similar
474 to *tap38, pgr5* shows lower LET and lower ΔETR(I) in HL, together with reduced ΔpH,
475 lower Y(ND), increased Y(NA) and PSI photoinhibition[22,58]. There is evidence that PGR5
476 might either act directly as part of a Fd-PQ reductase with PGRL1[8] or alternatively as a
477 regulatory element within a FNR-Fd-cytb_6f complex[10,78]. Thus, Fd reduction of PQ in HL
478 would be the limiting step in both *pgr5* and *tap38* mutants. Indeed, since the *pgr5* mutant also
479 fails to dephosphorylate LHCII in HL[79], and thus likely retains small grana in HL, it may be
480 crippled in two separate aspects of CET regulation.

481 The results in this study provide a basis for finally reconciling the role of LHCII
482 phosphorylation with regulation of CET. When the CBB cycle is limited by ATP in LL, the
483 resultant accumulation of NADPH and reduced Fd will increase Y(NA) and thus cause
484 reduction of the electron transfer chain upstream of PSI, including the PQ pool. STN7 is

activated by reduction of the PQ pool and LHCII phosphorylation triggers a transition to smaller grana and State II. Increased PSI excitation relative to PSII increases the rate of CET relative to LET and this provides extra ΔpH to increase ATP synthesis. In contrast in HL, when the CBB cycle is limited primarily by CO_2 availability, NADPH, reduced Fd *and* ATP accumulate. The latter factor is crucial since high ATP levels cause ΔpH to increase inhibiting STN7[18], despite the presence of a reduced PQ pool. The ensuing TAP38-dependent dephosphorylation LHCII triggers a transition to larger grana and State I, which facilitates increased CET by isolating the stromal PQ pool from PSII, poising it for CET. This synergy in the action of LHCII phosphorylation in LL and dephosphorylation in HL in promoting CET may be missing in green algae such as *Chlamydomonas*. To date dynamic thylakoid stacking changes have not yet been observed in *Chlamydomonas* and indeed the strict stacking of the membranes observed in higher plants is missing[80]. Another point of difference is that in *Chlamydomonas*, a supercomplex containing PSI, LHCII, cytb_6f, PGRL1, Fd and FNR is observed under conditions that promote CET[28,81]. It is possible that this CET supercomplex serves the same role as larger grana in higher plants, i.e. compartmentalising PQ for the CET pathway[81].

In conclusion, we have established that dynamic thylakoid stacking regulates photosynthetic electron transfer independent of state transitions, demonstrating they have a synergistic function in plants in regulating the PSI acceptor-side. Given the importance of STN7 to plant fitness [19–22] and since *tap38* plants were previously shown to grow faster than WT under controlled LL conditions[14], engineering crop plants to have constitutively high LHCII phosphorylation was considered a possible route to higher yield. However, our results show that dephosphorylation of LHCII serves a crucial photoprotective function in HL. Therefore, such a strategy is unlikely to yield success and a more nuanced approach is required.

Materials & Methods

Plant Material

Arabidopsis plants were grown for 5 weeks in a Conviron plant growth room with an 8-hour photoperiod at a light intensity of 200 µmol photons m^{-2} s^{-1} and day/night temperatures of 22/18 °C, respectively.

Structured illumination microscopy (SIM)

Arabidopsis was imaged on a DeltaVision OMX V4 microscope (GE Healthcare) equipped with the Blaze-3D SIM module and 60x 1.42 NA oil planapochromat lens. Chlorophyll fluorescence was excited with a 642 nm laser and the emission was collected through a 683/40 nm bandpass filter. The structured illumination pattern was projected onto the sample in a series of five phases for each of three angles leading to a total of 15 images per axial slice. The 3D image was acquired via sectioning with a 2D slice separation of 125 nm. The final super-resolution image was reconstructed with SoftWoRx OMX v6.0 software (GE Healthcare). Grana diameter was measured as the full-width half-maximum of a line profile across the granal-midpoint in images that had been thresholded and 16-bit converted with the SIMcheck plugin for ImageJ (v153).

Low-temperature fluorescence spectroscopy.

Thylakoid membranes were prepared according to Järvi *et al.*, 2011, from *Arabidopsis* leaves either adapted to LL (125 µmol photons m^{-2} s^{-1}) or HL (1150 µmol photons m^{-2} s^{-1}). 1 µM of chlorophyll from thylakoids was suspended in the fluorescence buffer (60% glycerol, 300 mM sucrose, 5 mM $MgCl_2$, 20 mM HEPES pH 7.8) and measured in 1 cm polymethyl methacrylate

cuvettes in a Opistat liquid nitrogen cooled bath cryostat (Oxford Instruments). Fluorescence emission measurements were performed as previously described using a FluoroLog FL3-22 spectrofluorimeter (Jobin Yvon)[32].

Spectroscopic determination of chlorophylls and cytochromes.

Spectroscopic assay of P700[83] and cytb_6f[84] content was performed on isolated thylakoids. Grana and stromal lamellae were prepared as described previously [85].

Gas exchange

A LICOR-6800 portable photosynthesis system was used to carry out infrared gas analysis (IRGA) on a fully expanded leaf while still attached to the plant. Relative humidity inside the IRGA chamber was kept at 60% to 65% using self-indicating desiccant, the flow rate was set at 150 µmol s^{-1}, and leaf temperature at 20°C. Reference [CO_2] was maintained at 400 ppm. After being matched, plants were allowed to equilibrate for 40 to 45 min inside the IRGA chamber. Once readings were stable, measurements were taken every 30 s for 10 min. Stomatal counts were performed as described[86].

Chlorophyll fluorescence and *in situ* P700, Pc and Fd absorption spectroscopy.

Pulse-amplitude modulated chlorophyll fluorescence and P700, Pc and Fd absorption spectroscopy were measured using a Dual-KLAS-NIR photosynthesis analyser (Walz) [42] or Imaging-PAM and associated software (v2.072). Maximum levels of Fd, Pc and P700 absorption were determined on leaves via induction of full oxidation (Pc, P700) or full reduction (Fd) and deconvolution by model spectra in NIR region [40,42,52]. For DIRK experiments the traces were normalised such that the maximally oxidised/reduced state (100%) was set using the maximum absorption obtainable using the method of Klughammer and Schreiber, 2016. Pc/P700 and Fd/P700 ratios (Extended Data Fig. 3) are represented as a relative values using the same procedure [42]. Chlorophyll fluorescence parameters and relative Pc, P700 and Fd redox state were determined at each light intensity using a 6 µmol photons s^{-1} m^{-2} modulated measuring light (540 nm) in combination with a saturating pulse of 18000 µmol photons m^{-2} s^{-1}. Actinic light was provided in the ratio of 10% 460 nm, 90% 635 nm. Far-red light (740nm), was provided at an intensity of 255 µmol photons m^{-2} s^{-1}. Chlorophyll fluorescence and P700 parameters were calculated as previously described [41,87]. The

estimated electron transport rate through PSI and PSII (ETR(I) and ETR (II)) was calculated using the formulae: ETR(I) = ΦPSI × I (light intensity) × PFDa (absorbed light) × PR (fraction light partitioned PSI), ETR(II) = ΦPSII × I (light intensity) × PFDa × PR (fraction light partitioned PSII). PFDa was calculated using an integrating sphere and PR from the data in Extended Data Fig. 1, applying the LL partition values to light intensities below 600 µmol photons m^{-2} $s^{-1}$and HL values to those above. The half-time for Pc, P700 and Fd redox changes was calculated by fitting a single exponential function to the DIRK (Fig. 3A-C) or flash data (Fig 4B, D)[45]. The initial slope (Fig. 3G, H, I) of DIRK was determined using a linear fit applied between 3 ms and 8 ms into the dark interval as this was determined to be a short enough window to give a reliable estimate (i.e. the slope was linear during this period (see Extended Data Fig. 4). The equilibrium constant (K_{eq}) for the forward reaction between the P700/$P700^+$ and Pc/Pc^+ redox couples is ~81 as calculated from their respective midpoint potentials (P700/$P700^+$ E'_m = 475 mV, Pc/Pc^+ E'_m = 362 mV) [55]. Compared to K_{eq} the apparent equilibrium constant (K_{app}) may be derived from the slope of the equilibrium plots derived from the DIRK data (Fig. 4C and Extended Data Fig. 5B)[40,42,52]. Single-turnover measurements (Fig. 4B, Extended Data Fig. 8A) were performed using a 50 µs flash (18000 µmol photons m^{-2} s^{-1}, 635 nm light), for Fig 4A a far-red background light (255 µmol photons m^{-2} s^{-1}, 740 nm) was also applied, 10 flashes per sample were averaged. Data analysed with Graphpad Prism v9.

ECS absorption spectroscopy.

The ECS signal was measured on leaves using a Walz Dual-PAM fitted with a P515/535 emitter module [48]. The proton conductance gH^+ (Extended Data Figs. 5C, 8B) and *pmf* (Fig. 4A, 5C) parameters were determined as previously described[88].

Infiltration

Leaves vacuum infiltrated with either 1mM methyl viologen (Fig 5B), 4 mM Iodoacetamide (IA) (Fig 5C and Extended Data Fig 6B), 30 µM 3-(3,4-dichlorophenyl)-1,1-dimethylurea (DCMU) (Extended Data Fig. 1 and Extended Data Fig. 8A) or 50 mM $NaNO_2$ (Fig. 5D and Extended Data Fig. 8C), buffered in 20 mM Hepes pH 7.5, 150 mM sorbitol, 50 mM NaCl (NaCl excluded for $NaNO_2$ infiltration).

Electron Microscopy

Thin-section EM was performed on leaves as previously described [33]

Data availability

The datasets analysed during the current study are available from the corresponding author on reasonable request. The sequence data from this article can be found in The Arabidopsis Information Resource or GenBank/EMBL database under the following accession numbers: STN7 (At1g68830), TAP38/PPH1 (At4t27800), CURT1A (At4g01150), CURT1B (At2g46820), CURT1C (At1g52220), CURT1D (At4g38100), PSAL (At4g12800).

Acknowledgments

We wish to thank Professor Dario Leister (LMU Munich) and Dr Mathias Pribil (Copenhagen Plant Science Center) for providing seeds of the *psal, curt1abcd*, oeCURT1A and *tap38* lines and Professor Lutz Eichacker (University of Stavenger) for providing seeds of *stn7*. Chris Hill (University of Sheffield) is acknowledged for assistance with the EM. M.P.J. acknowledges funding from the Leverhulme Trust grants RPG-2016-161 and RPG-2019-045 and the BBSRC White Rose DTP for a studentship to TEM (BB/M011151/1). The SIM imaging was performed at the University of Sheffield Wolfson Light Microscopy Facility and was partly funded by MRC Grant MR/K015753/1.

Author Contributions

M.P.J. and S.C. designed the study; C.H., W.H.J.W., T.Z.EM and M.S.P performed the research; C.H., W.H.J.W., T.Z.EM and M.P.J. analysed the data; M.P.J. C.H., W.H.J.W., T.Z.EM S.C. and M.S.P wrote the paper.

Ethics Declaration

Competing Interests

The authors declare no competing interests

References

1. Ruban, A. V. Evolution under the sun: Optimizing light harvesting in photosynthesis. *J. Exp. Bot.* (2015) doi:10.1093/jxb/eru400.
2. Miyake, C. Molecular mechanism of oxidation of p700 and suppression of ROS production in photosystem I in response to electron-sink limitations in C3 plants. *Antioxidants* **9**, 230 (2020).
3. Li, Z., Wakao, S., Fischer, B. B. & Niyogi, K. K. Sensing and Responding to Excess Light. *Annu. Rev. Plant Biol.* (2009) doi:10.1146/annurev.arplant.58.032806.103844.
4. Ruban, A. V., Johnson, M. P. & Duffy, C. D. P. The photoprotective molecular switch in the photosystem II antenna. *Biochim. Biophys. Acta - Bioenerg.* **1817**, 167–181 (2012).
5. Suorsa, M. *et al.* PGR5 ensures photosynthetic control to safeguard photosystem I under fluctuating light conditions. *Plant Signal. Behav.* e22741 (2013) doi:10.4161/psb.22741.
6. Johnson, G. N. Physiology of PSI cyclic electron transport in higher plants. *Biochim. Biophys. Acta - Bioenerg.* **1807**, 384–389 (2011).
7. Yamori, W. & Shikanai, T. Physiological Functions of Cyclic Electron Transport Around Photosystem I in Sustaining Photosynthesis and Plant Growth. *Annu. Rev. Plant Biol.* **67**, 81–106 (2016).
8. Hertle, A. P. *et al.* PGRL1 Is the Elusive Ferredoxin-Plastoquinone Reductase in Photosynthetic Cyclic Electron Flow. *Mol. Cell* (2013) doi:10.1016/j.molcel.2012.11.030.
9. Nandha, B., Finazzi, G., Joliot, P., Hald, S. & Johnson, G. N. The role of PGR5 in the redox poising of photosynthetic electron transport. *Biochim. Biophys. Acta - Bioenerg.* **1767**, 1252–1259 (2007).
10. Joliot, P. & Johnson, G. N. Regulation of cyclic and linear electron flow in higher Plants. *Proc. Natl. Acad. Sci. U. S. A.* **108**, 13317–13322 (2011).
11. Allen, J. F. State transitions - A question of balance. *Science* (2003)

653 doi:10.1126/science.1082833.
654 12. Ruban, A. V. & Johnson, M. P. Dynamics of higher plant photosystem cross-section
655 associated with state transitions. *Photosynth. Res.* **99**, 173–183 (2009).
656 13. Bellaflore, S., Barneche, F., Peltler, G. & Rochalx, J. D. State transitions and light
657 adaptation require chloroplast thylakoid protein kinase STN7. *Nature* **433**, 892–895
658 (2005).
659 14. Shapiguzov, A. *et al.* The PPH1 phosphatase is specifically involved in LHCII
660 dephosphorylation and state transitions in Arabidopsis. *Proc. Natl. Acad. Sci. U. S. A.*
661 (2010) doi:10.1073/pnas.0913810107.
662 15. Pribil, M., Pesaresi, P., Hertle, A., Barbato, R. & Leister, D. Role of plastid protein
663 phosphatase TAP38 in LHCII dephosphorylation and thylakoid electron flow. *PLoS*
664 *Biol.* (2010) doi:10.1371/journal.pbio.1000288.
665 16. Vener, A. V., Van Kan, P. J. M., Rich, P. R., Ohad, I. & Andersson, B. Plastoquinol at the
666 quinol oxidation site of reduced cytochrome bf mediates signal transduction between
667 light and protein phosphorylation: Thylakoid protein kinase deactivation by a single-
668 turnover flash. *Proc. Natl. Acad. Sci. U. S. A.* **94**, 1585–1590 (1997).
669 17. Rintamäki, E., Martinsuo, P., Pursiheimo, S. & Aro, E. M. Cooperative regulation of
670 light-harvesting complex II phosphorylation via the plastoquinol and ferredoxin-
671 thioredoxin system in chloroplasts. *Proc. Natl. Acad. Sci. U. S. A.* **97**, 11644–11649
672 (2000).
673 18. Fernyhough, P., Foyer, C. H. & Horton, P. Increase in the level of thylakoid protein
674 phosphorylation in maize mesophyll chloroplasts by decrease in the transthylakoid
675 pH gradient. *FEBS Lett.* **176**, 133–138 (1984).
676 19. Taylor, C. R., Van Ieperen, W. & Harbinson, J. Demonstration of a relationship
677 between state transitions and photosynthetic efficiency in a higher plant. *Biochem. J.*
678 (2019) doi:10.1042/BCJ20190576.
679 20. Frenkel, M. *et al.* Improper excess light energy dissipation in Arabidopsis results in a
680 metabolic reprogramming. *BMC Plant Biol.* (2009) doi:10.1186/1471-2229-9-12.
681 21. Külheim, C., Ågren, J. & Jansson, S. Rapid regulation of light harvesting and plant
682 fitness in the field. *Science (80-.).* **297**, 91–93 (2002).
683 22. Suorsa, M. *et al.* PROTON GRADIENT REGULATION5 is essential for proper acclimation
684 of Arabidopsis photosystem I to naturally and artificially fluctuating light conditions.

685 *Plant Cell* **24**, 2934–2948 (2012).
686 23. Lunde, C., Jensen, P. E., Haldrup, A., Knoetzel, J. & Scheller, H. V. The PSI-H subunit of
687 photosystem I is essential for state transitions in plant photosynthesis. *Nature* (2000)
688 doi:10.1038/35046121.
689 24. Fernyhough, P., Foyer, C. & Horton, P. The influence of metabolic state on the level of
690 phosphorylation of the light-harvesting chlorophyll-protein complex in chloroplasts
691 isolated from maize mesophyll. *BBA - Bioenerg.* (1983) doi:10.1016/0005-
692 2728(83)90235-9.
693 25. Allen, J. F. Protein phosphorylation - Carburettor of photosynthesis? *Trends Biochem.*
694 *Sci.* **8**, 369–373 (1983).
695 26. Cardol, P. *et al.* Impaired respiration discloses the physiological significance of state
696 transitions in Chlamydomonas. *Proc. Natl. Acad. Sci. U. S. A.* **15**, 15979–15984 (2009).
697 27. Bulté, L., Gans, P., Rebéillé, F. & Wollman, F. A. ATP control on state transitions in vivo
698 in Chlamydomonas reinhardtii. *BBA - Bioenerg.* (1990) doi:10.1016/0005-
699 2728(90)90095-L.
700 28. Takahashi, H., Clowez, S., Wollman, F. A., Vallon, O. & Rappaport, F. Cyclic electron
701 flow is redox-controlled but independent of state transition. *Nat. Commun.* **4**, 1954
702 (2013).
703 29. Pesaresi, P. *et al.* Arabidopsis STN7 kinase provides a link between short- and long-
704 term photosynthetic acclimation. *Plant Cell* **21**, 2402–2423 (2009).
705 30. Kyle, D. J., Staehelin, L. A. & Arntzen, C. J. Lateral mobility of the light-harvesting
706 complex in chloroplast membranes controls excitation energy distribution in higher
707 plants. *Arch. Biochem. Biophys.* **222**, 527–541 (1983).
708 31. Rozak, P. R., Seiser, R. M., Wacholtz, W. F. & Wise, R. R. Rapid, reversible alterations
709 in spinach thylakoid appression upon changes in light intensity. *Plant Cell Environ.*
710 (2002).
711 32. Wood, W. H. J., Barnett, S. F. H., Flannery, S., Hunter, C. N. & Johnson, M. P. Dynamic
712 thylakoid stacking is regulated by LHCII phosphorylation but not its interaction with
713 PSI. *Plant Physiol.* **180**, 2152–2166 (2019).
714 33. Wood, W. H. J. *et al.* Dynamic thylakoid stacking regulates the balance between linear
715 and cyclic photosynthetic electron transfer. *Nat. Plants* **4**, 116–127 (2018).
716 34. Anderson, J. M., Horton, P., Kim, E. H. & Chow, W. S. Towards elucidation of dynamic

structural changes of plant thylakoid architecture. *Philosophical Transactions of the Royal Society B: Biological Sciences* (2012) doi:10.1098/rstb.2012.0373.

35. Capretti, A. *et al.* Nanophotonics of higher-plant photosynthetic membranes. *Light Sci. Appl.* (2019) doi:10.1038/s41377-018-0116-8.

36. Grieco, M., Tikkanen, M., Paakkarinen, V., Kangasjärvi, S. & Aro, E. M. Steady-state phosphorylation of light-harvesting complex II proteins preserves photosystem I under fluctuating white light. *Plant Physiol.* **160**, 1896–1910 (2012).

37. Tikkanen, M., Grieco, M., Kangasjärvi, S. & Aro, E. M. Thylakoid protein phosphorylation in higher plant chloroplasts optimizes electron transfer under fluctuating light. *Plant Physiol.* (2010) doi:10.1104/pp.109.150250.

38. Tikkanen, M. *et al.* State transitions revisited—a buffering system for dynamic low light acclimation of Arabidopsis. *Plant Mol. Biol.* (2006) doi:10.1007/s11103-006-9088-9.

39. Pribil, M., Labs, M. & Leister, D. Structure and dynamics of thylakoids in land plants. *Journal of Experimental Botany* (2014) doi:10.1093/jxb/eru090.

40. Schreiber, U. & Klughammer, C. Analysis of photosystem I donor and acceptor sides with a new type of online-deconvoluting kinetic LED-array spectrophotometer. *Plant Cell Physiol.* (2016) doi:10.1093/pcp/pcw044.

41. Klughammer, C. & Schreiber, U. An improved method, using saturating light pulses, for the determination of photosystem I quantum yield via P700+-absorbance changes at 830 nm. *Planta* (1994) doi:10.1007/BF00194461.

42. Klughammer, C. & Schreiber, U. Deconvolution of ferredoxin, plastocyanin, and P700 transmittance changes in intact leaves with a new type of kinetic LED array spectrophotometer. *Photosynth. Res.* (2016) doi:10.1007/s11120-016-0219-0.

43. Sacksteder, C. A. & Kramer, D. M. Dark-interval relaxation kinetics (DIRK) of absorbance changes as a quantitative probe of steady-state electron transfer. *Photosynth. Res.* (2000) doi:10.1023/A:1010785912271.

44. Kirchhoff, H., Schöttler, M. A., Maurer, J. & Weis, E. Plastocyanin redox kinetics in spinach chloroplasts: Evidence for disequilibrium in the high potential chain. *Biochim. Biophys. Acta - Bioenerg.* **1659**, 63–72 (2004).

45. Ott, T., Clarke, J., Birks, K. & Johnson, G. Regulation of the photosynthetic electron transport chain. *Planta* (1999) doi:10.1007/s004250050629.

46. Jahns, P., Graf, M., Munekage, Y. & Shikanai, T. Single point mutation in the Rieske iron-sulfur subunit of cytochrome b6/f leads to an altered pH dependence of plastoquinol oxidation in Arabidopsis. *FEBS Lett.* **519**, 99–102 (2002).
47. Correa Galvis, V. *et al.* H + Transport by K + EXCHANGE ANTIPORTER3 Promotes Photosynthesis and Growth in Chloroplast ATP Synthase Mutants . *Plant Physiol.* (2020) doi:10.1104/pp.19.01561.
48. Klughammer, C., Siebke, K. & Schreiber, U. Continuous ECS-indicated recording of the proton-motive charge flux in leaves. *Photosynth. Res.* (2013) doi:10.1007/s11120-013-9884-4.
49. Sacksteder, C. A., Kanazawa, A., Jacoby, M. E. & Kramer, D. M. The proton to electron stoichiometry of steady-state photosynthesis in living plants: A proton-pumping Q cycle is continuously engaged. *Proc. Natl. Acad. Sci. U. S. A.* **97**, 14283–14288 (2000).
50. Johnson, M. P. & Ruban, A. V. Rethinking the existence of a steady-state Δψ component of the proton motive force across plant thylakoid membranes. *Photosynth. Res.* (2014) doi:10.1007/s11120-013-9817-2.
51. Armbruster, U. *et al.* Arabidopsis CURVATURE THYLAKOID1 proteins modify thylakoid architecture by inducing membrane curvature. *Plant Cell* (2013) doi:10.1105/tpc.113.113118.
52. Schreiber, U. Redox changes of ferredoxin, P700, and plastocyanin measured simultaneously in intact leaves. *Photosynth. Res.* (2017) doi:10.1007/s11120-017-0394-7.
53. Kirchhoff, H. *et al.* Dynamic control of protein diffusion within the granal thylakoid lumen. *Proc. Natl. Acad. Sci. U. S. A.* (2011) doi:10.1073/pnas.1104141109.
54. Joliot, P. & Joliot, A. Electron transfer between the two photosystems. II. Equilibrium constants. *BBA - Bioenerg.* (1984) doi:10.1016/0005-2728(84)90016-1.
55. Höhner, R. *et al.* Plastocyanin is the long-range electron carrier between photosystem II and photosystem I in plants. *Proc. Natl. Acad. Sci. U. S. A.* (2020) doi:10.1073/pnas.2005832117.
56. Kirchhoff, H., Horstmann, S. & Weis, E. Control of the photosynthetic electron transport by PQ diffusion microdomains in thylakoids of higher plants. *Biochim. Biophys. Acta - Bioenerg.* **1459**, 148–168 (2000).
57. Kirchhoff, H., Mukherjee, U. & Galla, H. J. Molecular architecture of the thylakoid

membrane: Lipid diffusion space for plastoquinone. *Biochemistry* (2002) doi:10.1021/bi011650y.

58. Yamamoto, H. & Shikanai, T. PGR5-dependent cyclic electron flow protects photosystem I under fluctuating light at donor and acceptor sides. *Plant Physiol.* **179**, 588–600 (2019).

59. Barbato, R. *et al.* Higher order photoprotection mutants reveal the importance of ΔpH-dependent photosynthesis-control in preventing light induced damage to both photosystem II and photosystem I. *Sci. Rep.* **10**, 1 (2020).

60. Kou, J., Takahashi, S., Fan, D. Y., Badger, M. R. & Chow, W. S. Partially dissecting the steady-state electron fluxes in photosystem I in wild-type and pgr5 and ndh mutants of arabidopsis. *Front. Plant Sci.* (2015) doi:10.3389/fpls.2015.00758.

61. Kadota, K. *et al.* Oxidation of P700 induces alternative electron flow in photosystem I in wheat leaves. *Plants* (2019) doi:10.3390/plants8060152.

62. Nawrocki, W. J. *et al.* Maximal cyclic electron flow rate is independent of PGRL1 in Chlamydomonas. *Biochim. Biophys. Acta - Bioenerg.* **1860**, 425–432 (2019).

63. Joliot, P. & Alric, J. Inhibition of CO2 fixation by iodoacetamide stimulates cyclic electron flow and non-photochemical quenching upon far-red illumination. *Photosynth. Res.* (2013) doi:10.1007/s11120-013-9826-1.

64. Nishio, J. N. & Whitmarsh, J. Dissipation of the proton electrochemical potential in intact chloroplasts. *Plant Physiol.* (1993) doi:10.1104/pp.101.1.89.

65. Joliot, P., Lavergne, J. & Béal, D. Plastoquinone compartmentation in chloroplasts. I. Evidence for domains with different rates of photo-reduction. *Biochim. Biophys. Acta - Bioenerg.* **1101**, 1–12 (1992).

66. Johnson, M. P., Vasilev, C., Olsen, J. D. & Hunter, C. N. Nanodomains of cytochrome b6f and photosystem II complexes in spinach grana thylakoid membranes. *Plant Cell* **26**, 3051–3061 (2014).

67. Tikhonov, A. N. The cytochrome b6f complex at the crossroad of photosynthetic electron transport pathways. *Plant Physiol. Biochem.* **81**, 163–183 (2014).

68. Schöttler, M. A. & Tóth, S. Z. Photosynthetic complex stoichiometry dynamics in higher plants: environmental acclimation and photosynthetic flux control. *Front. Plant Sci.* **5**, 188 (2014).

69. Pesaresi, P. *et al.* Mutants, overexpressors, and interactors of arabidopsis

plastocyanin isoforms: Revised roles of plastocyanin in photosynthetic electron flow and thylakoid redox state. *Mol. Plant* (2009) doi:10.1093/mp/ssn041.

70. Tiwari, A. *et al.* Photodamage of iron-sulphur clusters in photosystem i induces non-photochemical energy dissipation. *Nat. Plants* (2016) doi:10.1038/NPLANTS.2016.35.

71. Takagi, D. & Miyake, C. PROTON GRADIENT REGULATION 5 supports linear electron flow to oxidize photosystem I. *Physiol. Plant.* (2018) doi:10.1111/ppl.12723.

72. Foyer, C. H., Neukermans, J., Queval, G., Noctor, G. & Harbinson, J. Photosynthetic control of electron transport and the regulation of gene expression. *J. Exp. Bot.* **63**, 1637–1661 (2012).

73. Kramer, D. M. & Evans, J. R. The Importance of Energy Balance in Improving Photosynthetic Productivity. *Plant Physiol.* **155**, 70–78 (2011).

74. Munekage, Y. *et al.* Cyclic electron flow around photosystem I is essential for photosynthesis. *Nature* **429**, 579–582 (2004).

75. Giersch, C. *et al.* Energy charge, phosphorylation potential and proton motive force in chloroplasts. *BBA - Bioenerg.* (1980) doi:10.1016/0005-2728(80)90146-2.

76. Backhausen, J. E., Kitzmann, C., Horton, P. & Scheibe, R. Electron acceptors in isolated intact spinach chloroplasts act hierarchically to prevent over-reduction and competition for electrons. *Photosynth. Res.* (2000) doi:10.1023/A:1026523809147.

77. Slovacek, R. E., Mills, J. D. & Hind, G. The function of cyclic electron transport in photosynthesis. *FEBS Lett.* (1978) doi:10.1016/0014-5793(78)80136-7.

78. Buchert, F., Mosebach, L., Gäbelein, P. & Hippler, M. PGR5 is required for efficient Q cycle in the cytochrome b6f complex during cyclic electron flow. *Biochem. J.* **477**, 1631–1650 (2020).

79. Mekala, N. R., Suorsa, M., Rantala, M., Aro, E. M. & Tikkanen, M. Plants actively avoid state transitions upon changes in light intensity: Role of light-harvesting complex ii protein dephosphorylation in high light. *Plant Physiol.* **168**, 721–734 (2015).

80. Engel, B. D. *et al.* Native architecture of the chlamydomonas chloroplast revealed by in situ cryo-electron tomography. *Elife* (2015) doi:10.7554/eLife.04889.

81. Iwai, M. *et al.* Isolation of the elusive supercomplex that drives cyclic electron flow in photosynthesis. *Nature* **464**, 1210–1213 (2010).

82. Järvi, S., Suorsa, M., Paakkarinen, V. & Aro, E. M. Optimized native gel systems for separation of thylakoid protein complexes: Novel super- and mega-complexes.

Biochem. J. (2011) doi:10.1042/BJ20102155.

83. Melis, A. Kinetic analysis of P-700 photoconversion: Effect of secondary electron donation and plastocyanin inhibition. *Arch. Biochem. Biophys.* (1982) doi:10.1016/0003-9861(82)90535-5.

84. Metzger, S. U., Cramer, W. A. & Whitmarsh, J. Critical analysis of the extinction coefficient of chloroplasty cytochrome f. *Biochim. Biophys. Acta - Bioenerg.* (1997) doi:10.1016/S0005-2728(96)00164-8.

85. Fristedt, R. *et al.* Phosphorylation of photosystem II controls functional macroscopic folding of photosynthetic membranes in Arabidopsis. *Plant Cell* (2009) doi:10.1105/tpc.109.069435.

86. Hepworth, C., Doheny-Adams, T., Hunt, L., Cameron, D. D. & Gray, J. E. Manipulating stomatal density enhances drought tolerance without deleterious effect on nutrient uptake. *New Phytol.* (2015) doi:10.1111/nph.13598.

87. Maxwell, K. & Johnson, G. N. Chlorophyll fluorescence - A practical guide. *Journal of Experimental Botany* (2000) doi:10.1093/jxb/51.345.659.

88. Huang, W., Suorsa, M. & Zhang, S. B. In vivo regulation of thylakoid proton motive force in immature leaves. *Photosynth. Res.* (2018) doi:10.1007/s11120-018-0565-1.

89. Malkin, S., Armond, P. A., Mooney, H. A. & Fork, D. C. Photosystem II Photosynthetic Unit Sizes from Fluorescence Induction in Leaves. *Plant Physiol.* (1981) doi:10.1104/pp.67.3.570.

Figure legends

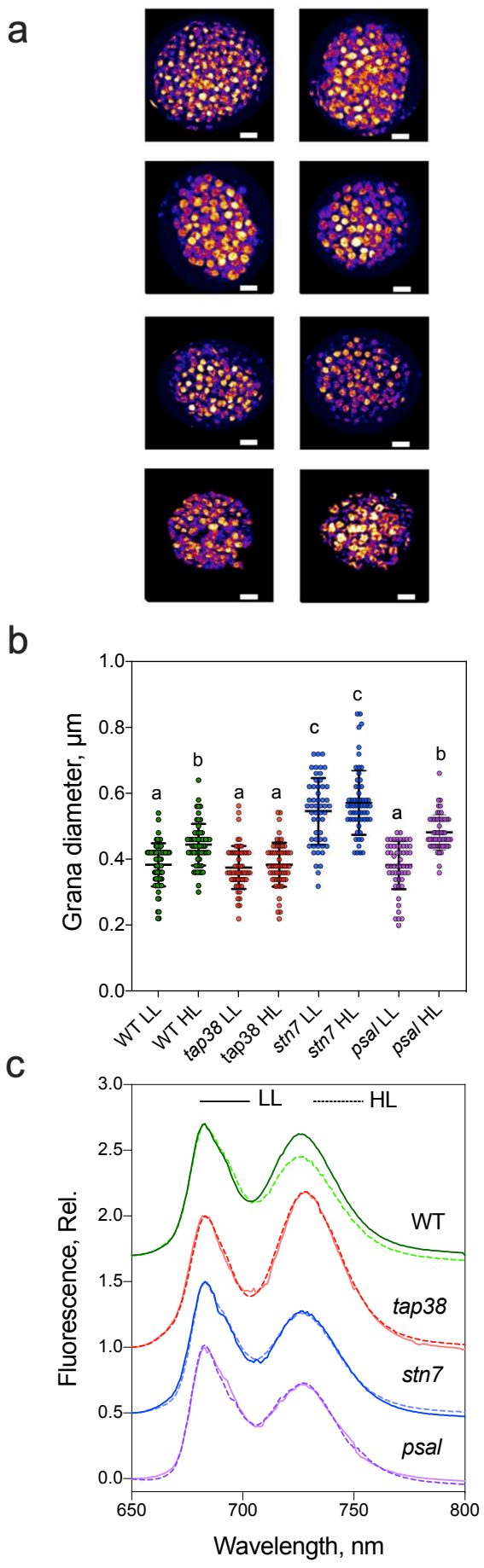
a
b
Grana diameter, µm
1.0
0.8
0.6
0.4
0.2
0.0
a
b
a
a
c
c
a
b
WT LL
WT HL
tap38 LL
tap38 HL
stn7 LL
stn7 HL
psaI LL
psaI HL
c
Fluorescence, Rel.
3.0
2.5
2.0
1.5
1.0
0.5
0.0
LL
HL
WT
tap38
stn7
psaI
650
700
750
800
Wavelength, nm

867

Figure 1 | Changes in thylakoid grana diameter and excitation energy distribution between photosystems in LL and HL. a, Representative SIM images of *Arabidopsis* WT, *stn7, tap38*, and *psal* mutants induced by 1 h of low light (LL, 125 µmol photons m^{-2} s^{-1}) or high light (HL, 1150 µmol photons m^{-2} s^{-1}), Scale bars 1 µm. Two independent sets of images were obtained with similar results. **b**, Mean grana diameter (FWHM of fluorescence signal) in each sample ± SD (n (number of grana analysed) = 66, 62, 54, 60, 60, 60, 55, 56 in order of presentation from left to right); the letters a, b and c represent significant differences calculated using one-way analysis of variance (ANOVA) with Tukey's multiple comparisons test, a-b P= 0.0001, a-c P=<0.0001, b-c P=<0.0001. **c**, Stacked 77 K fluorescence emission spectra (435 nm excitation) of thylakoids prepared from each sample following 1 h of LL (solid lines) or HL (dashed lines) treatment. Pairs of spectra (LL, HL) were normalised to 685 nm.

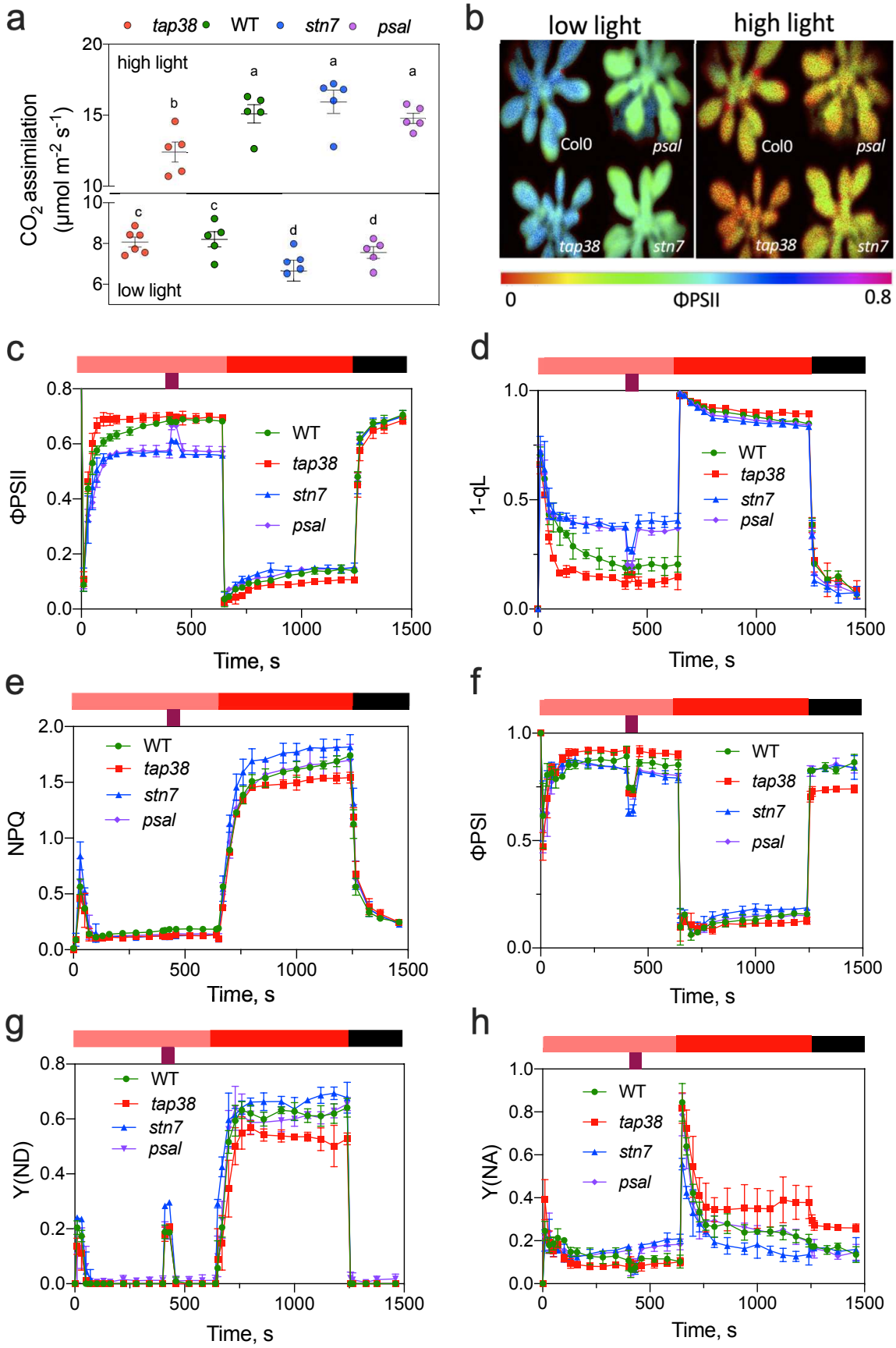
a
tap38
WT
stn7
psal
high light
low light
CO2 assimilation (µmol m-2 s-1)
b
low light
high light
Col0
psal
tap38
stn7
0
ΦPSII
0.8
c
ΦPSII
Time, s
d
1-qL
e
NPQ
f
ΦPSI
g
Y(ND)
h
Y(NA)

881

Figure 2 | Photosynthetic properties of WT, *tap38*, *stn7* and *psal Arabidopsis* plants determined by infra-red gas exchange, chlorophyll fluorescence and P700 absorption spectroscopy. a, CO_2 assimilation ($^{A}CO_2$) measured on each sample following 1 hour of low light (LL, 125 µmol photons m^{-2} s^{-1}) or high light (HL, 1150 µmol photons m^{-2} s^{-1}) illumination. The letters a, b, c and d represent significant differences calculated using one-way analysis of variance (ANOVA) with Tukey's multiple comparisons test, a-b P= 0.0009, a-c P=<0.0001, a-d P=<0.0001, b-c P=<0.0001, b-d P=<0.0001, c-d P=0.0009. **b**, Representative chlorophyll fluorescence images showing PSII quantum yield (ΦPSII) under LL and HL in each sample. **c**, Kinetics of ΦPSII under 10 minutes LL (pale red bar) including 30 s augmentation with far-red light (740 nm, 255 µmol photons m^{-2} s^{-1}, burgundy bar) and 10 minutes HL (bright red bar), followed by 4 minutes dark recovery in each sample (black bar). **d**, 1-qL (PSII acceptor side limitation), **e**, Non-photochemical quenching (NPQ), ***f***, Quantum yield of PSI (ΦPSI), **g**, PSI donor-side limitation (Y(ND)), **h**, PSI acceptor-side limitation (Y(NA)). n (separate plants analysed) = 5-6 for each sample; mean ± SD is shown for each timepoint.

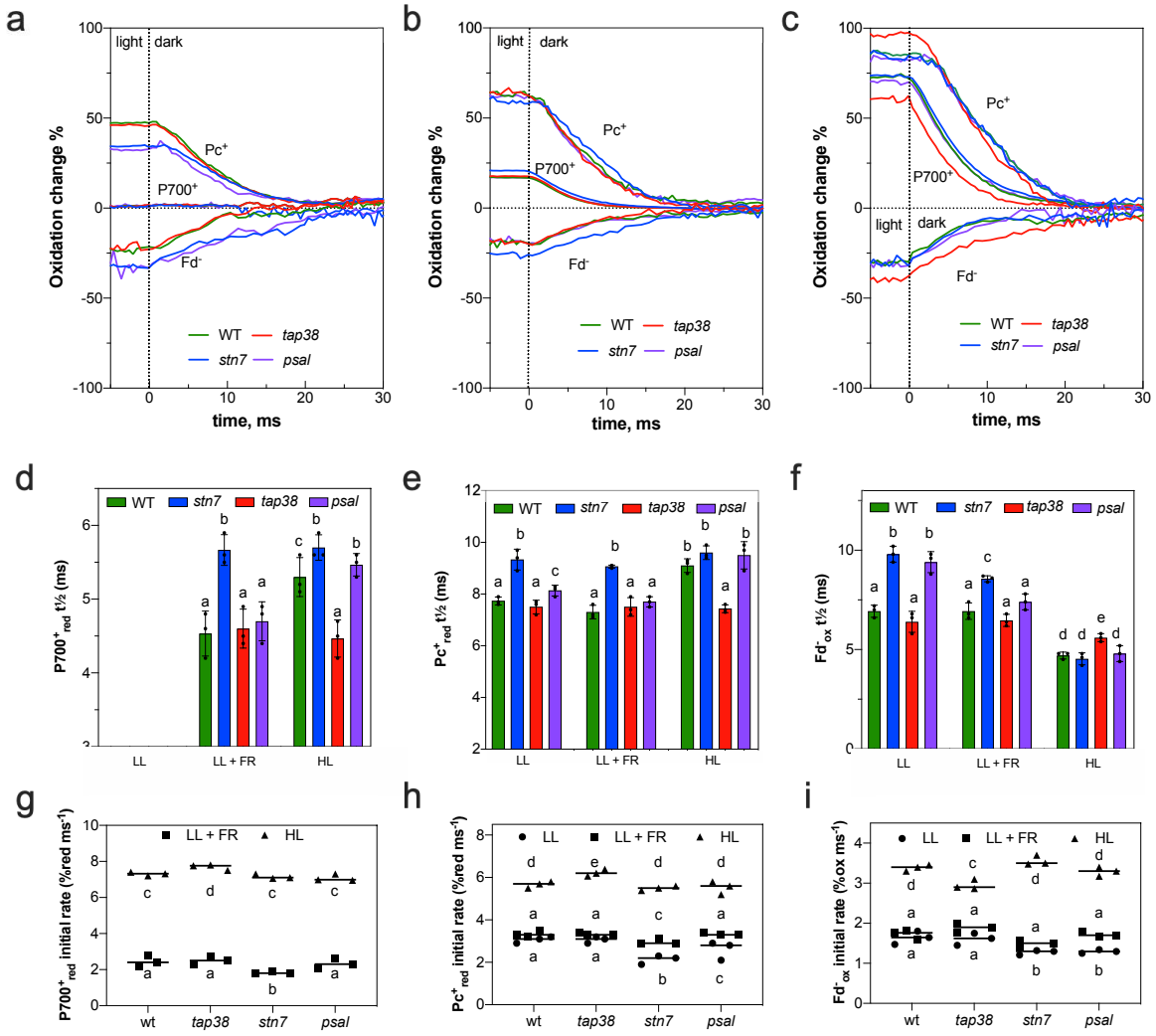

Figure 3 | Dark interval relaxation kinetic analysis of the reduction PSI ($P700^+$), Pc^+ and oxidation of Fd^-. **a**, DIRK analysis in leaves from each sample exposed to 10 minutes low light (LL, 125 µmol photons m^{-2} s^{-1}). **b**, DIRK analysis in leaves from each sample exposed to 10 minutes LL augmented for the final 30 seconds prior to dark interval with far-red light (740 nm, 255 µmol photons m^{-2} s^{-1}). **c**, DIRK analysis in leaves from each sample exposed to 10 minutes high light (HL, 1150 µmol photons m^{-2} s^{-1}). **d**, $P700^+$ reduction half-time calculated from single exponential fit of kinetics in a-c. The letters a-c represent significant differences calculated using one-way analysis of variance (ANOVA) with Tukey's multiple comparisons test, a-b P=<0.0001, a-c P=<0.0001, b-c P=0.0358. **e**, Pc^+ reduction half-time calculated from single exponential fit of kinetics in a-c. The letters a-c represent significant

differences calculated using one-way analysis of variance (ANOVA) with Tukey's multiple comparisons test, a-b P=<0.0001, a-c P=0.0106, b-c P=<0.0001. **f**, Fd^- oxidation half-time calculated from single exponential fit of kinetics in a-c. The letters a-e represent significant differences calculated using one-way analysis of variance (ANOVA) with Tukey's multiple comparisons test, a-b P=<0.0001, a-c P=0.0001, a-d P=<0.0001, a-e P=<0.0001, b-c P=0.046, b-d P=<0.0001, b-e P =<0.0001, c-d P=<0.0001, c-e P=<0.0001, d-e P=0.024. **g**, Initial rate of $P700^+$ reduction calculated from linear fit of kinetics in the 3-8 ms window in a-c. The letters a-d represent significant differences calculated using one-way analysis of variance (ANOVA) with Tukey's multiple comparisons test, a-b P=0.0001, a-c P=<0.0001, b-c P=<0.0001, b-d P=<0.0001, c-d P=0.008. **h**, Initial rate of Pc^+ reduction calculated from linear fit of kinetics in the 3-8 ms window in a-c. The letters a-d represent significant differences calculated using one-way analysis of variance (ANOVA) with Tukey's multiple comparisons test, a-b P=0.0001, a-c P=0.033, a-d P=<0.0001, a-e P=<0.0001, b-c P=0.027, b-d P=<0.0001, b-e P=<0.0001, c-d P=<0.0001, c-e P=<0.0001, d-e P=0.016. **i**, Initial rate of Fd^- oxidation calculated from linear fit of kinetics in the 3-8 ms window in a-c. The letters a-d represent significant differences calculated using one-way analysis of variance (ANOVA) with Tukey's multiple comparisons test, a-b P=0.038, a-c P=<0.0001, a-d P=<0.0001, b-c P=<0.0001, b-d P=<0.0001, c-d P=0.0001. n (separate plants analysed) = 3 for each sample in Fig 3; mean ± SD is shown.

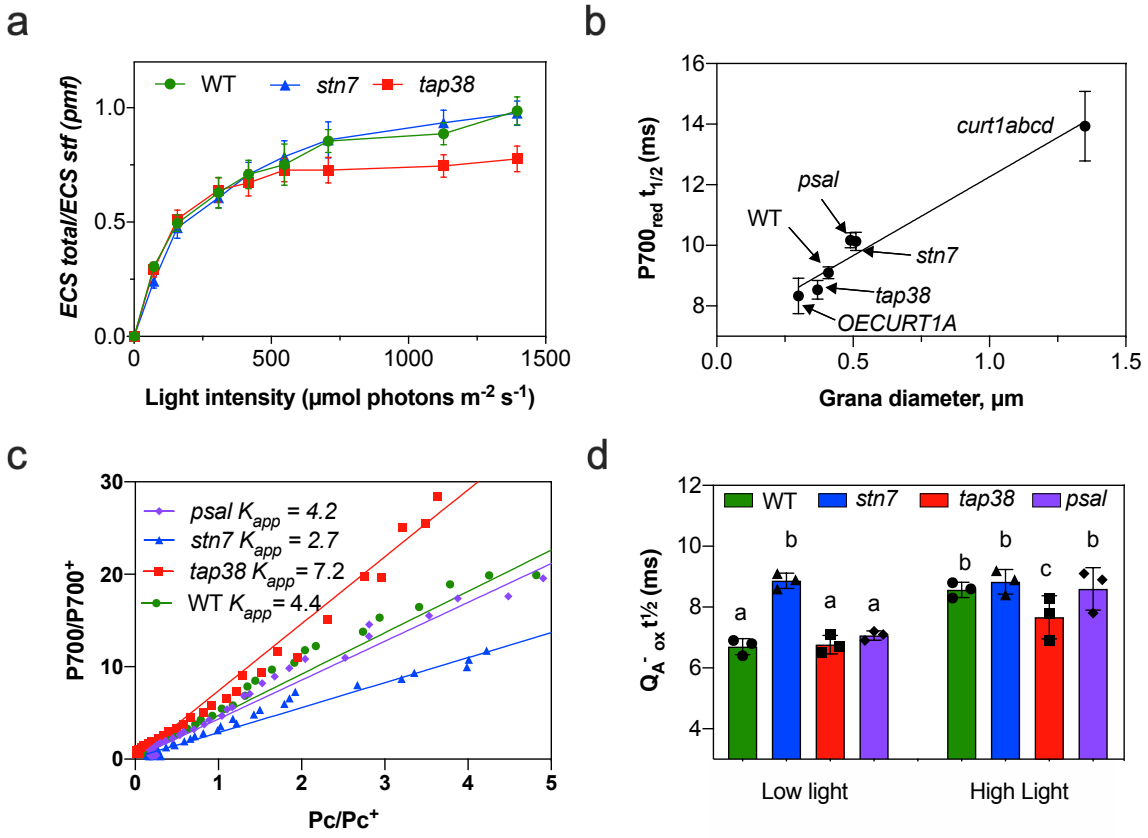

927

928 **Figure 4 | Investigating possible causes of defective electron transfer regulation in *stn7***
929 **and *tap38*. a,** Light-intensity dependence of total proton motive force (ECS total). The ECS
930 total levels were standardised against the 515-nm absorbance change induced by a single
931 turnover flash (ECS stf). **b**, Relationship between $P700^+$ reduction half-time following a
932 single-turnover flash (50 µs, 635 nm) applied on a far-red light background (740 nm, 255
933 µmol photons m^{-2} s^{-1}). **c**, Equilibrium plot of $P700/P700^+$ versus Pc/Pc^+ from dark interval
934 relaxation kinetics after high light treatment shown in Fig 3C. Apparent equilibrium constants
935 (K_{app}) were calculated from a linear fit of the slope, R values for the linear fits were WT =
936 0.968, *stn7* = 0.982, *tap38* = 0.973 and *psal* 0.974 . **d**, Q_A^- oxidation half-time derived from
937 decay of PSII chlorophyll fluorescence signal following a 200 ms saturating pulse applied to
938 leaves treated for 1 hour with low light (125 µmol photons m^{-2} s^{-1}) or high light (1150 µmol
939 photons m^{-2} s^{-1}). The letters a-d represent significant differences calculated using one-way
940 analysis of variance (ANOVA) with Tukey's multiple comparisons test, a-b P=<0.0001, a-c

P=<0.0001, b-c P=0.012. n (separate plants analysed) = 3 for each sample in Fig 4; mean ± SD is shown.

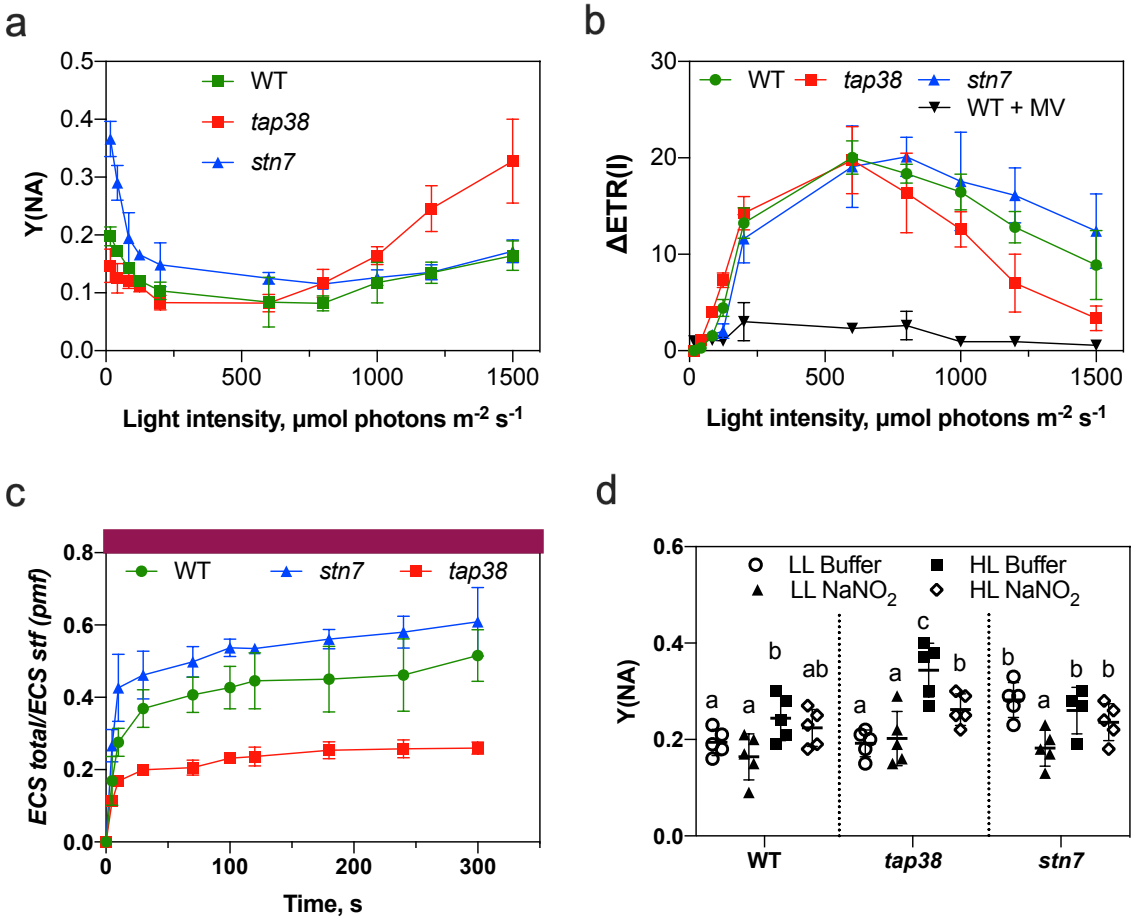

Figure 5 | Comparison of PSI acceptor side limitation and cyclic electron transfer. a, Light-intensity dependence of PSI acceptor side limitation (Y(NA)). n (separate plants analysed) = 3 for each sample; mean ± SD is shown for each point. **b**, Light-intensity dependence of the difference in estimated electron transfer rate between PSI and PSII (ΔETR(I) = ETR(I)-ETR(II)). n (separate plants analysed) = 5-6 for each sample; mean ± SD is shown for each point. **c**, Kinetics of proton motive force formation (ECS total) induced by 5 minutes illumination with far-red light (740 nm, 255 µmol photons m^{-2} s^{-1}, burgundy bar) on leaves infiltrated with 4mM iodoacetamide. n (separate plants analysed) = 3 for each sample; mean ± SD is shown for each point. The ECS total levels were standardised against the 515-nm absorbance change induced by a single turnover flash (ECS stf). **d**, Y(NA) after

10 minutes illumination in low light (LL, 125 µmol photons m^{-2} s^{-1}) or high light (HL, 1150 µmol photons m^{-2} s^{-1}) in leaves infiltrated with either 20 mM Hepes pH 7.5, 150 mM sorbitol, 50 mM NaCl (buffer) or buffer with NaCl replaced by 50 mM $NaNO_2$. n (separate plants analysed) = 5 for each sample; mean ± SD is shown for each point. The letters a-d represent significant differences calculated using one-way analysis of variance (ANOVA) with Tukey's multiple comparisons test, a-b P=0.0001, a-c P=<0.0001, b-c P=<0.0001.